Biosphere model simulations of interannual variability in terrestrial $^{13}C/^{12}C$ exchange

I. R. van der Velde,[1] J. B. Miller,[2,3] K. Schaefer,[4] K. A. Masarie,[2] S. Denning,[5] J. W. C. White,[6] P. P. Tans,[2] M. C. Krol,[1,7] and W. Peters[1]

Received 4 April 2012; revised 6 May 2013; accepted 15 May 2013; published 8 July 2013.

[1] Previous studies suggest that a large part of the variability in the atmospheric ratio of $^{13}CO_2/^{12}CO_2$ originates from carbon exchange with the terrestrial biosphere rather than with the oceans. Since this variability is used to quantitatively partition the total carbon sink, we here investigate the contribution of interannual variability (IAV) in biospheric exchange to the observed atmospheric ^{13}C variations. We use the Simple Biosphere - Carnegie-Ames-Stanford Approach biogeochemical model, including a detailed isotopic fractionation scheme, separate ^{12}C and ^{13}C biogeochemical pools, and satellite-observed fire disturbances. This model of $^{12}CO_2$ and $^{13}CO_2$ thus also produces return fluxes of $^{13}CO_2$ from its differently aged pools, contributing to the so-called disequilibrium flux. Our simulated terrestrial ^{13}C budget closely resembles previously published model results for plant discrimination and disequilibrium fluxes and similarly suggests that variations in C_3 discrimination and year-to-year variations in C_3 and C_4 productivity are the main drivers of their IAV. But the year-to-year variability in the isotopic disequilibrium flux is much lower ($1\sigma = \pm 1.5$ PgC ‰ yr^{-1}) than required (± 12.5 PgC ‰ yr^{-1}) to match atmospheric observations, under the common assumption of low variability in net ocean CO_2 fluxes. This contrasts with earlier published results. It is currently unclear how to increase IAV in these drivers suggesting that SiBCASA still misses processes that enhance variability in plant discrimination and relative C_3/C_4 productivity. Alternatively, ^{13}C budget terms other than terrestrial disequilibrium fluxes, including possibly the atmospheric growth rate, must have significantly different IAV in order to close the atmospheric ^{13}C budget on a year-to-year basis.

Citation: van der Velde, I. R., J. B. Miller, K. Schaefer, K. A. Masarie, S. Denning, J. W. C. White, P. P. Tans, M. C. Krol, and W. Peters (2013), Biosphere model simulations of interannual variability in terrestrial $^{13}C/^{12}C$ exchange, *Global Biogeochem. Cycles*, *27*, 637–649, doi:10.1002/gbc.20048.

1. Introduction

[2] Measured atmospheric CO_2 and its $^{13}C/^{12}C$ ratio (expressed as $\delta^{13}C$ in ‰) are complementary and have been combined to estimate net oceanic and terrestrial exchange at the Earth's surface [e.g., *Tans et al.*, 1993; *Ciais et al.*, 1995; *Francey et al.*, 1995; *Fung et al.*, 1997; *Joos and Bruno*, 1998; *Rayner et al.*, 2008]. The ratio of the ^{13}C and ^{12}C stable isotopes provide an additional constraint on the net global carbon uptake from the atmosphere by either the terrestrial biosphere or by the ocean, given that each flux discriminates slightly differently against the heavier ^{13}C isotope of CO_2. This process is called "isotopic fractionation" or discrimination and gives terrestrial and oceanic carbon exchange its own isotopic signature and its own distinct influence on the atmospheric $\delta^{13}C$ ratio.

[3] But the use of atmospheric $\delta^{13}C$ to partition the ocean and land uptake requires reasonably detailed knowledge of other processes in the ^{13}C budget. Special attention must for instance be directed to the isotopic disequilibrium flux [*Tans*, 1980; *Tans et al.*, 1993], which stems from differences in isotopic composition between "old" carbon released from oceanic and terrestrial reservoirs and the current atmosphere. The continuing depletion of atmospheric $\delta^{13}C$ by

[1]Meteorology and Air Quality, Wageningen University, Wageningen, The Netherlands.
[2]NOAA Earth System Research Laboratory, Boulder, Colorado, USA.
[3]CIRES, University of Colorado, Boulder, Colorado, USA.
[4]National Snow and Ice Data Center, University of Colorado, Boulder, Colorado, USA.
[5]Department of Atmospheric Science, Colorado State University, Fort Collins, Colorado, USA.
[6]INSTAAR, University of Colorado, Boulder, Colorado, USA.
[7]IMAU, Utrecht University, Utrecht, The Netherlands.

Corresponding author: I. R. van der Velde, Meteorology and Air Quality, Wageningen University, P.O. Box 47 6700 AA Wageningen, The Netherlands. (ivar.vandervelde@wur.nl)

0886-6236/13/10.1002/gbc.20048

the addition of ^{13}C depleted fossil CO_2 (also known as the Suess effect; *Suess* [1955]) causes the atmosphere to be relatively isotopically light compared to the "old" carbon that is released from the reservoirs. In addition to this low-frequency component of disequilibrium flux, year-to-year changes in fractionation resulting from either C_3-only and/or C_3:C_4 productivity changes can induce interannual variability (IAV) in disequilibrium flux [e.g., *Scholze et al.*, 2008; *Alden et al.*, 2010].

[4] Close attention must also be paid to seasonal and spatial variations of C_3 and C_4 plant isotopic fractionation. Variations in C_3 fractionation are controlled by stomatal opening and closing, which are typically modeled as being driven by leaf-atmosphere water vapor gradients. Fractionation during photosynthesis can be accounted for by simulating the leaf interior CO_2 as a function of assimilation and stomatal conductance, as in the studies of *Lloyd and Farquhar* [1994] and *Fung et al.* [1997]. In recent studies, more detailed process descriptions have been used to estimate plant fractionation [e.g., *Kaplan et al.*, 2002; *Suits et al.*, 2005; *Scholze et al.*, 2003, 2008]. *Scholze et al.* [2003, 2008] developed in the Lund-Potsdam-Jena dynamic vegetational model (LPJ), a terrestrial cycling framework of CO_2 and $^{13}CO_2$ that included year-to-year changes in both isotopic fractionation and disequilibrium fluxes. They found that IAV in ^{13}C exchange was controlled by fractionation changes caused by climate variability and productivity (GPP) shifts between areas dominated by C_3 or C_4 vegetation. Fires and land use change contributed only on the longer time scales, which are relevant for the disequilibrium fluxes. If these were ignored, though, the partitioning of net carbon fluxes from atmospheric CO_2 and $\delta^{13}C$ in a traditional "double-deconvolution" [e.g., *Ciais et al.*, 1995] method would change by 1 PgC yr^{-1}.

[5] When isotopic fractionation and low-frequency disequilibrium fluxes (and fossil fuel emissions) are properly accounted for, double deconvolution (separating land and ocean uptake based on CO_2 and $\delta^{13}C$ observations) can be a method for separating the average net ocean and net land uptake fluxes over longer time scales. In contrast, the year-to-year variability on these estimated net fluxes is more problematic: when only net biosphere and net ocean fluxes are estimated in a double deconvolution, the resulting IAV on ocean fluxes is much larger than bottom-up ocean models support [*Winguth et al.*, 1994; *Le Quere et al.*, 2003]. This unrealistically large ocean variability anticorrelates with the estimated IAV in terrestrial fluxes from this method, which are needed to match the observed variability in $\delta^{13}C$. *Alden et al.* [2010] recently addressed this unrealistic outcome of the IAV in traditional double-deconvolution estimates and suggested that under the common assumption of low IAV of ocean exchange, the terrestrial disequilibrium flux instead could be given large IAV to match the year-to-year changes in the atmospheric $\delta^{13}C$. Thus, the ocean and terrestrial biosphere net flux variability would be identical to our best estimates from CO_2-only based estimates and process model simulations. This explanation of atmospheric $\delta^{13}C$ variability from *Alden et al.*, along with the traditional one from *Ciais et al.*, is visually illustrated in Figure 1b and further explained in section 3.1. In addition, *Randerson et al.* [2002] suggested that if IAV in terrestrial C_3 fractionation covaries with IAV in GPP (e.g., better growth conditions along with stronger fractionation), smaller year-to-year changes in net ocean and land fluxes are needed to explain the atmospheric $\delta^{13}C$ variability.

[6] In this study, we examine the extent to which these previous findings by *Alden et al.* [2010], *Randerson et al.* [2002], and *Scholze et al.* [2003] are supported by a new bottom-up terrestrial biosphere model. Like the model of *Scholze et al.* [2008], it incorporates a detailed description of the exchange of ^{12}C and ^{13}C with the atmosphere from hourly to decadal time scales. We specifically focus our analysis on the interannual variability of the ^{13}C fluxes produced by our model and what they imply for the variability of net terrestrial CO_2 fluxes if we try to close the $^{13}C/^{12}C$ budgets in a double-deconvolution approach. Inevitably, this warrants a closer look at the IAV of the terrestrial disequilibrium flux because of its key role in this estimation and supposed large variability [*Alden et al.*, 2010]. But can the terrestrial biosphere really cause that much variability (research question 1)? Can the covariation between GPP and terrestrial isotopic fractionation indeed contribute to atmospheric $\delta^{13}C$ variability as suggested by *Randerson et al.* [2002] (research question 2)? And if not, then what process should be reconsidered to close the ^{13}C budget from the point of view of interannual variability (research question 3)?

2. Methodology

2.1. SiBCASA Model

[7] Previous efforts led to the development of the SiBCASA model, which combines photosynthesis and biophysical processes from the SiB (Simple Biosphere) model version 3 with carbon biogeochemical processes from the Carnegie-Ames-Stanford Approach model [*Schaefer et al.*, 2008]. Meteorological driver data are provided by the European Centre for Medium-Range Weather Forecasting (ECMWF) from 2000 up to 2008. SiBCASA calculates at 10 min time steps and on a spatial resolution of $1° \times 1°$ the surface energy, water, and CO_2 fluxes and predicts the moisture content and temperature of the canopy and soil [*Sellers et al.*, 1996]. In an iterative process, the uptake of carbon is calculated by the Ball-Berry stomatal conductance model [*Collatz et al.*, 1991] in combination with a C_3 enzyme kinetic model [*Farquhar et al.*, 1980] and a C_4 photosynthesis model [*Collatz et al.*, 1992]. Subsequently, the CO_2 concentration ratio between the leaf chloroplast and atmosphere is determined in this coupled framework.

[8] These ratios are further used in a modified version of the fractionation scheme [*Farquhar*, 1983; *Lloyd and Farquhar*, 1994; *Suits et al.*, 2005] to calculate at each time step a gradient-weighted C_3 plant fractionation factor Δ_{C3}:

$$\Delta_{C_3} = \Delta_b\left(\frac{C_a - C_s}{C_a}\right) + \Delta_s\left(\frac{C_s - C_i}{C_a}\right) + \left(\Delta_{diss} + \Delta_{aq}\right)\left(\frac{C_i - C_c}{C_a}\right) + \Delta_f\left(\frac{C_c}{C_a}\right), \quad (1)$$

where the C's represent the partial pressures of CO_2 at canopy air space (C_a), leaf boundary layer (C_s), leaf stomata (C_i), and chloroplast (C_c). The isotopic fractionation effects (Δ) represent the relative reduction of ^{13}C to ^{12}C at different uptake stages from canopy air space to leaf chloroplasts. These stages are as follows: CO_2 diffusion from C_a to C_s

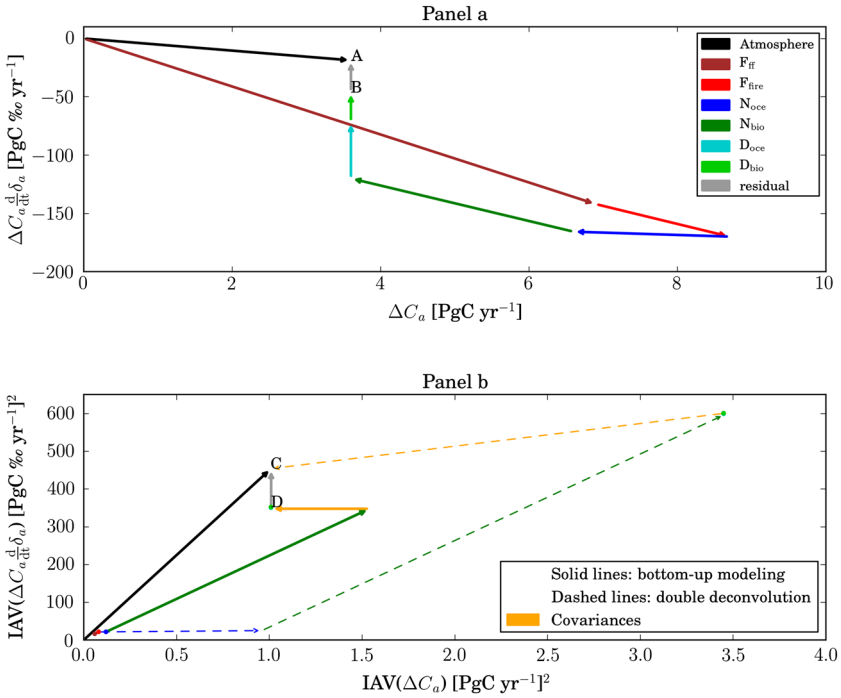

Figure 1. (a) The vector plot of the average rate of change of CO_2 and $\delta^{13}C$ observed in the atmosphere (black vector pointing to A) and the contributions from the different bottom-up terms from equations (2) and (4) (add up to point B). The gap between A and B represents the missing mean 27.1 PgC ‰ yr^{-1} isoflux in the $\delta^{13}C$ budget, which could be accounted for by scaling D_{bio} and D_{oce}. (b) The vector plot of the IAV ($1\sigma^2$) in the fluxes. Again, observed IAV is depicted by the black vector pointing to C, and the colored vectors (pointing to D) represent the different terms of the CO_2 and $\delta^{13}C$ budgets. The smallest terms of the budget are presented as dots. Covariances, largely due to anticorrelation between N_{bio} and N_{oce}, are depicted by the orange vectors. Moving the model representation of IAV at point D toward observed IAV at point C requires either (1) more IAV in the disequilibrium fluxes, shown by the solid vectors, or (2) more IAV in the land and ocean uptake fluxes shown by the dashed vectors. For the discrimination and terrestrial disequilibrium fluxes, we used SiBCASA's ISOVAR simulation.

(Δ_b = 2.9‰) and CO_2 diffusion through C_i (Δ_s = 4.4‰), dissolution of CO_2 in mesophyll, and transport to the chloroplast (Δ_{diss} = 1.1 and Δ_{aq} = 0.7‰, respectively). However, the largest isotope effect (i.e., the strongest reduction of ^{13}C relative to ^{12}C) is associated with the fixation of CO_2 by the enzyme RuBisCO in the chloroplast (Δ_f = 28.2‰). C_4 plant discrimination was held constant at $\Delta_{C4} = \Delta_s$ = 4.4‰, and no discrimination was assigned to the respiration fluxes. The time invariant C_3/C_4 plant distribution map is determined from ecosystem modeling, satellite data, and maps of agriculture [*Still et al.*, 2003].

[9] In the CASA part of the model [*Randerson et al.*, 1996], we set up 13 biogeochemical pools for total carbon ($^{12}C + ^{13}C$) and ^{13}C separately. The assimilated carbon and ^{13}C are added to two separate storage pools and become available for plant growth. In subsequent stages, the carbon is propagated to their own separate live carbon pools, surface litter pools, and layered soil pools. For each pool, the carbon stocks are solved as a first-order linear differential equation depending on gains from other pools, losses to other pools, and respiration losses due to (heterotrophic) microbial decay and (autotrophic) plant growth [*Schaefer et al.*, 2008]. SiBCASA now has a semiprognostic canopy, which means that the leaf pool is prognostic, but the photosynthesis calculations are constrained by remotely sensed absorbed fraction of photosynthetically active radiation (fPAR). No discrimination effects are considered for transfers of carbon between pools. The average turnover times, as well as the scaling factors for temperature, freezing, and moisture, were taken from the original CASA scheme.

[10] The SiBCASA fire emissions (CO_2 and $^{13}CO_2$) follow the methodology of *van der Werf et al.* [2003, 2010]. The estimated fire emissions are driven by multiple remotely sensed burned area products combined in the Global Fire Emissions Database (GFED) version 3.1 [*Giglio et al.*, 2010]. Only above ground, fine litter pools and coarse woody debris at the surface were subject to combustion. Peat burning [*Page et al.*, 2002] and organic soil carbon combustion were not taken into account for this publication. The global averaged biomass burning flux for the period 1991–2007 amounts to 1.82 ± 0.17 PgC yr^{-1}, which is similar to the value of 2.0 PgC yr^{-1} published by *van der Werf et al.* [2010].

2.2. Mass Balance of Atmospheric CO_2 and $^{13}CO_2$

[11] Atmospheric CO_2 and $^{13}CO_2$ mole fractions reflect the sum of several flux terms at the Earth's surface, and they can be expressed by two mass balance equations:

$$\frac{d}{dt}C_a = F_{ff} + F_{fire} + N_{bio} + N_{oce}, \quad (2)$$

$$\frac{d}{dt}{}^{13}C_a = {}^{13}F_{ff} + {}^{13}F_{fire} + {}^{13}N_{bio} + {}^{13}N_{oce}, \quad (3)$$

where C_a represents the mole fraction of atmospheric CO_2, N_{bio} and N_{oce} are the net CO_2 exchange fluxes in the terrestrial biosphere and oceans, F_{ff} represents the CO_2 emission due to fossil fuel combustion and cement production, and F_{fire} represents the CO_2 emission due to biomass burning. The $^{13}CO_2$ counterparts are labeled with 13. Because both atmospheric CO_2 and $^{13}CO_2$ are conserved quantities, equations (2) and (3) can be manipulated following *Tans et al.* [1993] and give a budget equation expressed as the rate of change of atmospheric $\delta^{13}C$ (henceforth δ_a):

$$\begin{aligned} C_a \frac{d}{dt}\delta_a = {} & F_{ff}(\delta_{ff} - \delta_a) + F_{fire}(\delta_{ab} - \delta_a) && \text{[emission forcing terms]} \\ & + N_{bio}(\delta_{ab} - \delta_a) + N_{oce}(\delta_{ao} - \delta_a) && \text{[net exchange forcing terms]} \\ & + F_{ba}(\delta_{ba} - \delta_{ab}) + F_{fire}(\delta_{fire} - \delta_{ab}) && \text{[terrestrial disequilibrium forcing terms]} \\ & + F_{oa}(\delta_{oa} - \delta_{ao}) && \text{[ocean disequilibrium forcing term].} \end{aligned} \quad (4)$$

[12] The subscripts ab, ba, ao, and oa denote the direction of the one-way gross fluxes and isotopic signatures, e.g., F_{ba} refers to the autotrophic and heterotrophic respiration fluxes from the terrestrial biosphere to the atmosphere. The isotopic signatures of the CO_2 fluxes (δ_{xx}) are expressed as ‰ deviation relative to the Vienna Pee Dee Belemnite. Negative δ's indicate that the $^{13}C/^{12}C$ ratio of a given sample is smaller than the VPDB standard. In assimilated carbon, the isotopic signature (δ_{ab}) is formulated by

$$\delta_{ab} = 1000 \times \left(\frac{{}^{13}F_{ab}/{}^{12}F_{ab}}{({}^{13}C/{}^{12}C)_{std}} - 1 \right) \approx \delta_a - \Delta. \quad (5)$$

The signatures of the other fluxes are calculated in the same way, e.g., δ_{ba} is calculated by taking the ratio of the ^{13}C and ^{12}C fluxes of F_{ba} and reflects the long-term integrated effects of the changes in atmospheric isotopic composition, in GPP, in fractionation, in carbon storage, and in respiration.

[13] Note that we split up the term $F_{fire}(\delta_{fire} - \delta_a)$ into two separate terms: $F_{fire}(\delta_{ab} - \delta_a)$ and $F_{fire}(\delta_{fire} - \delta_{ab})$. The latter term quantifies the influence of biomass burning to the disequilibrium flux, whereas the former term includes biomass burning as part of the terrestrial net flux, which scales with terrestrial fractionation. The main advantage of writing the isotopic ratio of the fire flux in such a way is that it allows for calculating δ_{fire} directly from the ratio of the ^{13}C and ^{12}C fluxes of F_{fire} rather than using an approximation (δ_{ba}).

[14] Equation (4) allows us to distinguish the changes in the atmospheric isotopic ratios brought by (1) the discrimination processes during the net CO_2 exchange in the terrestrial biosphere and oceans and (2) by an isotopic disparity between the release and uptake of CO_2 at Earth's surface. As explained in section 1, we are particularly interested if the *simulated* interannual variability (IAV) on the right-hand side of the equation can balance the *measured* variability on the left-hand side. Incorrect IAV in disequilibrium flux, combined with that observed in the atmosphere, can lead to wrongly projected variability in net land and, therefore by residual, in net ocean fluxes.

[15] The global quantities of CO_2 and $\delta^{13}C$ are derived from a large collection of sampling sites in the Cooperative Air Sampling Network of the National Oceanic and Atmospheric Administration/Earth System Research Laboratory (NOAA/ESRL). The isotopic analysis of each sample is performed at the University of Colorado Institute of Arctic and Alpine Research/Stable Isotope Lab (INSTAAR/SIL).

[16] The IAV in the terrestrial disequilibrium forcing terms of equation (4) simulated in SiBCASA is mainly due to changes in discrimination and shifts in C_3 and C_4 productivity propagating into the carbon pools and then reemerging as respired CO_2 and fire CO_2. The mean flux is the consequence of a long-term draw down of the atmospheric $^{13}C/^{12}C$ ratio due to fossil fuel emissions of isotopically light CO_2. That makes the older carbon that is released to the atmosphere richer in ^{13}C compared to the carbon that is currently taken up by the sinks. For the terrestrial biosphere, this isotopic difference is designated as the isodisequilibrium forcing coefficient [*Alden et al.*, 2010] and is separately defined for biological respiration $I_{ba} = \delta_{ba} - \delta_{ab}$ and for biomass burning $I_{fire} = \delta_{fire} - \delta_{ab}$. It has a strong control on the budget equation because the isodisequilibrium coefficient scales with large gross fluxes [*Alden et al.*, 2010]. The total isotopic disequilibrium flux from the terrestrial biosphere D_{bio} is the following:

$$\begin{aligned} D_{bio} &= F_{ba}[\delta_{ba} - \delta_{ab}] + F_{fire}[\delta_{fire} - \delta_{ab}] \\ &= F_{ba}I_{ba} + F_{fire}I_{fire}. \end{aligned} \quad (6)$$

The global area-weighted averaged D_{bio} in PgC ‰ yr^{-1} is calculated using SiBCASA output variables:

$$D_{bio} = \left[\sum_{x=1}^{n} F_{ba}[x] \cdot (\delta_{ba}[x] - \delta_{ab}[x]) \cdot GA[x] + \sum_{x=1}^{n} F_{fire}[x] \cdot (\delta_{fire}[x] - \delta_{ab}[x]) \cdot GA[x] \right] \times UC, \quad (7)$$

where the fluxes $F_{ba}[x]$ and $F_{fire}[x]$ for each grid cell x are given in μmol m^{-2} s^{-1}, where n represents the total number of land grid cells, where $GA[x]$ is the grid area in m^2 for each grid cell x, and UC is a unit conversion factor to convert from μmol ‰ s^{-1} to PgC ‰ yr^{-1}.

[17] Other sources of annual fluxes and isotopic signatures in equation (4) are the following: (1) F_{ff} and δ_{ff}, compiled from the Carbon Dioxide Information and Analysis Center [*Boden et al.*, 2009] and British Petrol Statistical Review of World Energy June (2009); (2) F_{fire}, estimated by SiBCASA; (3) N_{oce}, estimated by *Le Quere et al.* [2007]; (4) ocean fractionation $\epsilon \approx (\delta_{ao} - \delta_a)$, kept constant at –2‰ [*Zhang et al.*, 1995]; (5) N_{bio}, the estimated residual from equation (2); and (6) bottom-up ocean disequilibrium flux D_{oce} [*Alden et al.*, 2010].

2.3. Reynolds Decomposition on D_{bio}

[18] Our third research question (which processes contribute most to variability in terrestrial disequilibrium?) requires a way to separate the yearly fluctuations from the

Table 1. Description of the Four Different Simulations

Name Simulation	Variable C_3 Fractionation	Variable δ_a	Fire	Run Time
ISOVAR	+	+	+	1851–2008
ISOFIX	fixed at 19.2‰	+	+	1851–2008
ISOFIX-FA (fixed atmosphere)	fixed at 19.2‰	fixed δ_a	+	ISOFIX restart from 1975
ISOVAR-NF (no fires)	+	+	–	1851–2008

trend for each process that contributes to D_{bio} in equation (6), e.g., F_{ba}, I_{ba}, or I_{fire}. One technique to achieve this separation is Reynolds decomposition, where for a certain quantity x, the fluctuating part is separated from the mean: i.e., $x = x' + \bar{x}$ [*Reynolds*, 1895]. Applying a Reynolds decomposition on equation (6) gives us in total eight terms:

$$\overline{D}_{bio} + D'_{bio} = \overline{F}_{ba}\overline{I}_{ba} + \overline{F}_{ba}I'_{ba} + F'_{ba}\overline{I}_{ba} + F'_{ba}I'_{ba} + \overline{F}_{fire}\overline{I}_{fire} + \overline{F}_{fire}I'_{fire} + F'_{fire}\overline{I}_{fire} + F'_{fire}I'_{fire}. \quad (8)$$

To let D'_{bio} represent the year-to-year changes on short time scales rather than decadal changes in the mean, we let $\overline{D}_{bio}$ include a linear trend over a time period (for this study, 1991–2007). Although the sum of the eight Reynolds terms characterize D_{bio} completely, the total *variance* in D_{bio} is equal to the sum of variances of each of the eight terms plus all their possible covariances according to the following:

$$\mathrm{VAR}(D_{bio}) = \sum_{i=1}^{8}\sum_{j=1}^{8}\mathrm{COV}(X_iX_j). \quad (9)$$

Applying this to equation (8) gives a total of 64 (co-)variance terms. These terms placed in a covariance matrix allows us a quick analysis of the major contributing terms of the total variability, both the variance of the single terms, as well as the covariances between terms. With the summation of the appropriate terms, we can isolate specific drivers of variability in D_{bio}. For instance, the variance caused by changes only in the isodisequilibrium coefficient ($\overline{F}_{ba}I'_{ba}$) is expressed by the diagonal variance term. Any other covariances between ($\overline{F}_{ba}I'_{ba}$) and other terms can be obtained by adding up the off-diagonal covariances. By dividing VAR($\overline{F}_{ba}I'_{ba}$) by VAR(D_{bio}), we can also obtain its relative contribution to the total variance in %. In a similar way, this method also allows separation of variance of other contributors.

2.4. Experimental Setup

[19] We ran SiBCASA globally, for each simulation, from 1851 through 2008. The initial carbon pool sizes are analytically solved by setting the time derivatives of the pools to zero. This approximation implies biospheric steady state (net ecosystem CO_2 exchange (NEE) $\approx$ 0), and this assumption is often made for biogeochemical models since observations of biomass are not available [*Schaefer et al.*, 2008]. Our data sets combined (meteorology, remotely sensed vegetation data, and GFED3) allowed a model run with actual driver data for the period 2000 through 2008. For each model year from 1851–1999, the meteorological and GFED3 burned area data were randomly selected from the 2000–2008 data set. Therefore, our framework excluded any variability from long-term climate change effects such as a rise in global temperature. However, the records of atmospheric δ_a and CO_2 concentration did have a realistic long-term trend. The monthly δ_a record, as a function of latitude, was based on ice core measurements [*Francey et al.*, 1999] and from 1989 onward on atmospheric observations (ftp://ftp.cmdl.noaa.gov/ccg/co2c13). The long-term trend of atmospheric CO_2 was taken from curve fit of the global CO_2 concentration and included observed seasonal cycles derived at sites in the Northern Hemisphere, near equator, and Southern Hemisphere.

[20] In this study, we performed four different simulations (Table 1). All simulations included the prescribed records of atmospheric CO_2 and δ_a, the same C_3/C_4 distribution map, and the same SiBCASA driver files as described earlier. The ISOVAR simulation (we borrowed the same terminology as *Scholze et al.* [2003, 2008]) included the dynamic fractionation scheme, whereas the ISOFIX simulation used fixed values for C_3 and C_4 plant discrimination (19.2 and 4.4‰, respectively) instead. In addition, the ISOFIX simulation was also restarted from 1975 onward with fixed δ_a to investigate the variability induced by atmospheric $^{13}C/^{12}C$ ratios (ISOFIX-FA, Fixed Atmosphere). To investigate to what extent the exclusion of fire disturbances will increase the D_{bio} flux, we ran a fourth simulation. This simulation was similar to ISOVAR but lacked the fire fluxes (ISOVAR-NF, No Fires), where total NEE remained unaffected because the excluded fire disturbances were compensated by increased respiration.

3. Results

3.1. Total $\delta^{13}C$ Budget

[21] We first address the question whether simulated terrestrial flux IAV can close simultaneously the CO_2 and $\delta^{13}C$ budget under the assumption of low ocean flux IAV. Thereto, we assume a closed CO_2 budget (equation (2) and Table 2), given the rate of change of CO_2, the rate of fossil fuel combustion, the rate of biomass burning, and the ocean exchange to be known, and thus assign the remainder of budget to terrestrial net exchange (mean and IAV). The solution to this "single deconvolution" is shown graphically in Figure 2a, and increases in CO_2 from F_{ff} and F_{fire} are partly countered by uptake in the terrestrial biosphere and oceans. The remainder of the emitted CO_2 accumulates on average with 3.6 PgC yr^{-1} in the atmosphere. Note that the residual term of –0.53 (PgC yr^{-1})^2 in the IAV represents the sum of the remaining covariances between the fluxes. This value is largely the result of negative covariances (anticorrelations) between N_{bio} and F_{ff} and between N_{bio} and N_{oce}. There is, however, no physical basis for it, but it is simply the result of closing the CO_2 balance.

[22] When filling the budget terms on the right-hand side of equation (4) with values from SiBCASA and from other estimates, we obtain a sum of the mean isofluxes of $^{13}CO_2$ that requires an additional $\sim$27 PgC ‰ yr^{-1} to match the left-hand side (see Table 2). In addition, we miss totally 102

Table 2. The 1991–2007 Averaged Observed Records of $C_a d/dt\delta_a$ and d/dtC_a Balanced by the Flux Terms Defined by Equations (2) and (4). The Mass Balance of CO_2 and $\delta^{13}C$ Include Columns Containing the Standard Deviation (1σ) and the Variance ($1\sigma^2$), Respectively, of the Linear Detrended IAV. Other Adopted Values, Which Are Also Averaged Over 1991–2007, Are Given in the Most Right-Hand Side Columns. Footnotes Provide the Sources of the Data

Mass Balance $\delta^{13}C$ Budget (PgC ‰ yr^{-1})				Mass Balance C Budget (PgC yr^{-1})				Other Adopted Values	
	Mean	1σ	$1\sigma^2$		Mean	1σ	$1\sigma^2$		Mean
$C_a d/dt\delta_a$ [a]	–18.7	±21.32	454.41	d/dtC_a [a]	3.6	±1.00	1.01	δ_a [a]	–8.0‰
$F_{ff}(\delta_{ff}-\delta_a)$	–141.9	±4.00	16.00	F_{ff} [e]	6.9	±0.24	0.06	δ_{ff} [e]	–28.6‰
$F_{fire}(\delta_{ab}-\delta_a)$	–27.8	±2.30	5.28	F_{fire} [f]	1.8	±0.15	0.02	$(\delta_{ab}-\delta_a)=-\Delta$ [i]	–15.2‰
$N_{oce}(\delta_{ao}-\delta_a)$	4.2	±0.37	0.14	N_{oce} [g]	–2.1	±0.19	0.04	$(\delta_{ao}-\delta_a)=\epsilon$ [j]	–2.0‰
$N_{bio}(\delta_{ab}-\delta_a)$	45.6	±18.07	326.52	N_{bio} [h]	–3.0	±1.19	1.42	C_a [a]	779.2 PgC
D_{bio} [b]	25.4	±1.46	2.14	covariances [d]			–0.53	$d/dt\delta_a$ [a]	–0.024‰ yr^{-1}
D_{oce} [c]	48.7	±1.48	2.21						
residual [d]	27.1	±10.11	102.12						

[a]Observed global average derived from the Cooperative Air Sampling Network of NOAA/ESRL and INSTAAR/SIL.
[b]Global average calculated from SiBCASA's records of F_{ba}, δ_{ab} and δ_{ba}.
[c]Global average calculated from observed records of pCO_2 and $\delta^{13}C$ in dissolved inorganic carbon, and estimated F_{oa}.
[d]Leftover residuals to close the CO_2 and $\delta^{13}C$ budgets (equations (2) and (4)).
[e]Global average compiled from CDIAC and British Petrol Statistical Review of World Energy.
[f]Global average calculated by SiBCASA biomass burning module.
[g]Global average estimated by *Le Quere et al.* [2007].
[h]Global average estimated by closing the average carbon budget (equation (2)).
[i]Difference between assimilated isotopic signature and atmospheric isotopic signature is assumed equal to SiBCASA's fractionation power Δ (equation (5)).
[j]Difference between ocean dissolved isotopic signature and atmospheric isotopic signature is assumed equal to ocean fractionation (ϵ).

$\left[\text{PgC ‰ yr}^{-1}\right]^2$ of IAV in the simulated budget, of which 138 $\left[\text{PgC ‰ yr}^{-1}\right]^2$ is present in the residual term and –36 $\left[\text{PgC‰yr}^{-1}\right]^2$ is present in the remainder of the covariances between the fluxes. Although 102 $\left[\text{PgC‰yr}^{-1}\right]^2$ seems like a large missing fraction, closer inspection points to only a few processes that dominate the budget and thus could be held responsible. We illustrate this in Figure 2b with numerical values again in Table 2.

[23] The mean observed $\delta^{13}C$ growth rate ($C_a d/dt \quad \delta_a$) is negative (black line) and shows a considerable amount of variability (*mean* ± 1σ *detrended standard deviation*: –18.7 ± 21.3 PgC ‰ yr^{-1}). The negative sign in the mean flux implies that the atmosphere gets more and more depleted in $^{13}CO_2$ relative to $^{12}CO_2$. On the mean flux side, combustion of isotopically light fossil fuels (brown shaded) dominates this drawdown, with small contribution from fires (red shaded). As calculated, neither one of these terms has much variability, but the fire contribution (–27.8 ± 2.3 PgC ‰ yr^{-1}) may be a little more variable than simulated in SiBCASA because of its intermittent nature and capacity to shift between C_3 and C_4 dominated ecosystems with large consequences for its signature.

[24] The sum of these two negative terms (∼–170 PgC ‰ yr^{-1}) is partly balanced by four positive flux terms that tend to increase the ratio of $^{13}CO_2$ and $^{12}CO_2$ in the atmosphere. Of these four fluxes, the ocean disequilibrium term (light blue) has the strongest impact on the balance but is also estimated to have only small IAV (48.7 ± 1.5 PgC ‰ yr^{-1}). This large flux is a result of large gross CO_2 fluxes toward the atmosphere and the relatively large isotopic difference between $\delta^{13}C$ in the surface ocean and atmosphere. The role of net CO_2 exchange in the oceans (blue) is small (4.2 ± 0.4 PgC ‰ yr^{-1}) because of the low IAV in ocean model simulations and the assumed constant fractionation of –2‰.

[25] Exchange with the terrestrial biosphere also contributes through a net flux and a disequilibrium term. The net terrestrial biosphere CO_2 exchange (green) contributes strongly to the mean isoflux and also causes large IAV in simulated isofluxes (45.6 ± 18.1 PgC ‰ yr^{-1}). The terrestrial disequilibrium D_{bio} is important for the mean budget, but we find that it exhibits quite low IAV (25.4 ± 1.5 PgC ‰ yr^{-1}) even when variations in C_3 discrimination and changes in C_3:C_4 productivity are included (ISOVAR). When excluded, the variability reduces even further to ±1.2 PgC ‰ yr^{-1} (ISOFIX).

[26] So what is wrong with this simulated budget that misses 27.1 ± 10.1 PgC ‰ yr^{-1} of isofluxes? Vector diagrams of the CO_2 and $\delta^{13}C$ budgets (Figure 1) provide us some visual aid to recognize which of the terms can provide extra leverage. Point A in Figure 1a represents the growth rate that is measured in the atmosphere that we are trying to match, but adding up all the bottom-up terms gets us only up to point B, i.e., 27.1 PgC ‰ yr^{-1} less than needed to close the budget. The disequilibrium fluxes do not affect the CO_2 budget; hence, they only appear as vertical vectors. So, moving from B to A can be done relatively easy if we scale the vertical ocean and land disequilibrium vectors as done in *Alden et al.* [2010]. This can be justified by the

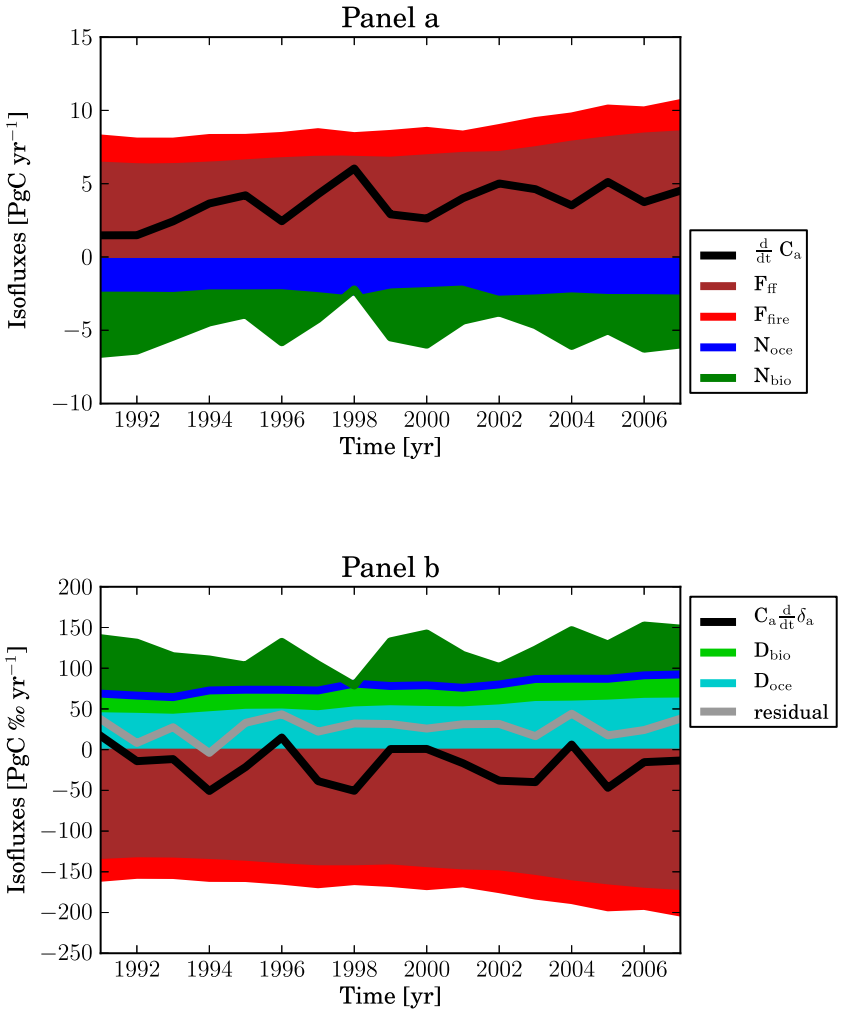

Figure 2. Time series of each term of the (a) CO_2 budget equation (2) and (b) $\delta^{13}C$ budget equation (4). The global annual isofluxes (right-hand side of the equations) are plotted as stacked area time series. Global annual observed d/dtC_a and C_ad/dtδ_a (left-hand side of the equations) are plotted as a black line, and the global annual residual isoflux is plotted as a gray line. For the discrimination and terrestrial disequilibrium fluxes, we used SiBCASA's ISOVAR simulation.

realization that the processes that determine these fluxes, especially on land, are still uncertain. The gross CO_2 fluxes toward the atmosphere and the turnover times of the carbon pools as simulated in SiBCASA are not constrained by observations. More problematic, though, is the fraction of variability that our simulations cannot account for in the budget. In Figure 1b, point C represents the IAV that is observed in the atmosphere, but again we fall short with our bottom-up framework and end at point D, around 100 $\left[\text{PgC‰yr}^{-1}\right]^2$ too low. Note that F_{ff} and N_{oce} only have a small influence on the IAV budget (their arrows are packed tightly together in the lower left corner) so adjustments to these fluxes will hardly help close the variability gap. F_{fire} might provide some additional variability given the lack of specific burning events in Indonesia and elsewhere but is likely not enough to close the budget. In contrast, N_{bio} has a large influence on $\delta^{13}C$ IAV but in a standard double-deconvolution method N_{bio} cannot be adjusted without a change in N_{oce}. So to close the budget (moving from D to C), we can choose two solutions: (1) to assume all missing IAV to reside in D_{oce}, or more likely in D_{bio}, as was done by *Alden et al.* [2010], or (2) to project all unexplained IAV onto the net uptake fluxes, as shown by the dashed vectors and done in *Ciais et al.* [1995]. Solution 1 seems the easiest but is not supported by our current bottom-up modeling as we will show in the next section. Solution 2, on the other hand, gives unrealistically large (and anticorrelating; r = –0.7) IAV in both ocean and land uptake, but this solution is not supported by bottom-up modeling of net ocean fluxes [e.g., *Le Quere et al.*, 2007]. In section 4, we will analyze the implications of this outcome and suggest possible alternative ways to close the budget. But first, we will examine our terrestrial disequilibrium flux in more detail and answer our second and third research questions.

3.2. Variability in Terrestrial Fluxes

[27] The results from our Reynolds decomposition applied on terrestrial disequilibrium flux (D_{bio}, equation (8)) of the ISOVAR simulation is summarized graphically in Figure 3 in the form of a covariance matrix, of which we

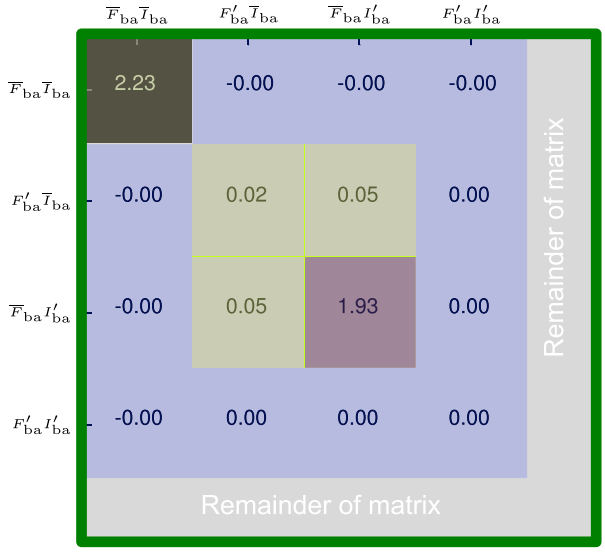

Figure 3. The outcome of Reynolds decomposition (equation (8)) applied to a covariance matrix. The sum of the whole matrix equals the total IAV in D_{bio} and is indicated by the green border. We let the mean fluxes and disequilibrium coefficients include a linear trend over the period investigated (1991–2007). Therefore, in our summations, we exclude the terms (black box) between the mean terms because they provide no information about year-to-year variations. The sum of the gray area represents only a small portion of the total IAV, which is mainly caused by covariances between biomass burning and biological respiration (off-diagonal terms). Everything inside the blue area represents the IAV caused by biological respiration. Contributions are further dissected between $I_{ba}{}'$ (purple) and a selection of the remainder terms (light green).

show only the important contributing terms. The summations of different terms are painted with different colors and reappear in the schematic overview of the important variability contributions (Figure 4). The sum of the complete matrix gives the detrended year-to-year variability in D_{bio} ($2.13\ \left[\text{PgC‰yr}^{-1}\right]^2$, or ± 1.46 PgC ‰ yr^{-1}). Three quarters of the complete covariance matrix is responsible for only 4% of the total variability and is therefore omitted from Figure 3. Our results suggest that the variability in terrestrial disequilibrium results nearly completely (96%) from respiration-driven disequilibrium ($F_{ba}I_{ba}$), while fire-driven disequilibrium ($F_{fire}I_{fire}$) has a negligible impact (4%). With only a small fire flux of 1.8 PgC yr^{-1} and similarly small variability (± 0.2 PgC yr^{-1} 1σ), this result was expected. The contribution from fires can potentially be enhanced by higher fire emissions during El Niño events (e.g., 1997–1998), but in SiBCASA, we do not simulate all process, like peat burning, thought to contribute to additional high fire emissions. Even if we would have more IAV in the fire flux, it will likely not affect the total disequilibrium flux that much. The year-to-year changes in the fire isodisequilibrium coefficient scale only with a fire flux of 2 to 3 PgC/yr, whereas changes in the respiration isodisequilibrium coefficient scale with a much large respiration flux. Despite the small size of the variability, there is a significant ~10% impact of fires on global total disequilibrium because fires shorten the residence time of carbon in the biosphere and hence decrease the difference between respired carbon and assimilated carbon. This mostly affects tropical fluxes, where fires are more predominant and residence times are generally longer than for C_4 herbaceous plant species. Between 1991 and 2007, the ISOVAR-NF simulation had a global average D_{bio} flux of 27.1 PgC ‰ yr^{-1} instead of 25.4 PgC ‰ yr^{-1} in the standard ISOVAR simulation.

[28] From the 96% of respiration-driven IAV in disequilibrium, only 6% comes from IAV in the respiration flux F_{ba} (green), and 90% comes from IAV in the disequilibrium forcing coefficient I_{ba} (purple). This agrees well with the conclusions of *Scholze et al.* [2008] and of *Alden et al.* [2010], who also ascribe terrestrial disequilibrium variability to the isotopic forcing rather than the respiration variations. Physically, this is consistent with the idea that the large terrestrial carbon pools from which respiration emerges limit the degree to which it can vary. Variability in I_{ba} is further decomposed in three parts: (1) 19% of variability in I_{ba} results from variations in global averaging of the discrimination factor Δ as the relative uptake (GPP) over C_3 vegetated areas (with large Δ_{C3}) and C_4 (with small Δ_{C4}) vegetated areas shifts. For example, a 0.5% relative increase of C_4 GPP causes a 0.08‰ reduction in global average Δ. (2) 48% results from variations in the atmospheric *delta*$_a$, which together with the global Δ determines δ_{ab}, and (3) another 33% comes from changes in Δ_{C3}, which is the second contributor to global Δ and was assumed to vary only in C_3 plants and acted mostly as a short-term response to drought conditions. This latter contribution was excluded in the ISOFIX simulation, and its variability in our simulations is slightly smaller than in *Scholze et al.* [2003]. In contrast, our simulations show larger variations in the C_3/C_4 contributions to global Δ instead of Δ_{C3}. Comparing against the total variability in D_{bio}, the three contributors in I_{ba} together represent 90% of the variability with the following relative contributions: (1) 17%, (2) 43%, and (3) 30%.

[29] Because the variability from D_{bio} is rather low, much of the terrestrial variability originates from the net exchange flux (N_{bio}), as we have seen in the previous section. An interesting aspect is that less IAV in N_{bio} and N_{oce} is required to explain the observed year-to-year changes in atmospheric CO_2 and $\delta^{13}C$ if GPP and plant discrimination covary in response to drought stress. This idea was first presented by *Randerson et al.* [2002], who assumed that a 1% increase in GPP would result in a 0.5% increase in discrimination when solving their double-deconvolution setup. This resulted in a substantial reduction of the minimum to maximum range of the yearly terrestrial and ocean carbon sinks (0.7 PgC yr^{-1} and 0.4 PgC yr^{-1}, respectively), compared to a double deconvolution with constant discrimination.

[30] In SiBCASA, the drought responses of C_3 GPP and fractionation are included in the model itself, as increases in vapor pressure deficit and water stress tend to close the leaf stomata. This reduces GPP and the daytime chloroplast-atmosphere (C_c/C_a) ratio and, hence, simultaneously reduces Δ_{C3} through equation (1). We find that linearly detrended C_3 GPP and Δ_{C3} do indeed covary ($r = +0.6$) as hypothesized by *Randerson et al.* [2002], but only 10% of the total variability in the isoflux ($F_{C3ab}\Delta_{C3}$) comes from

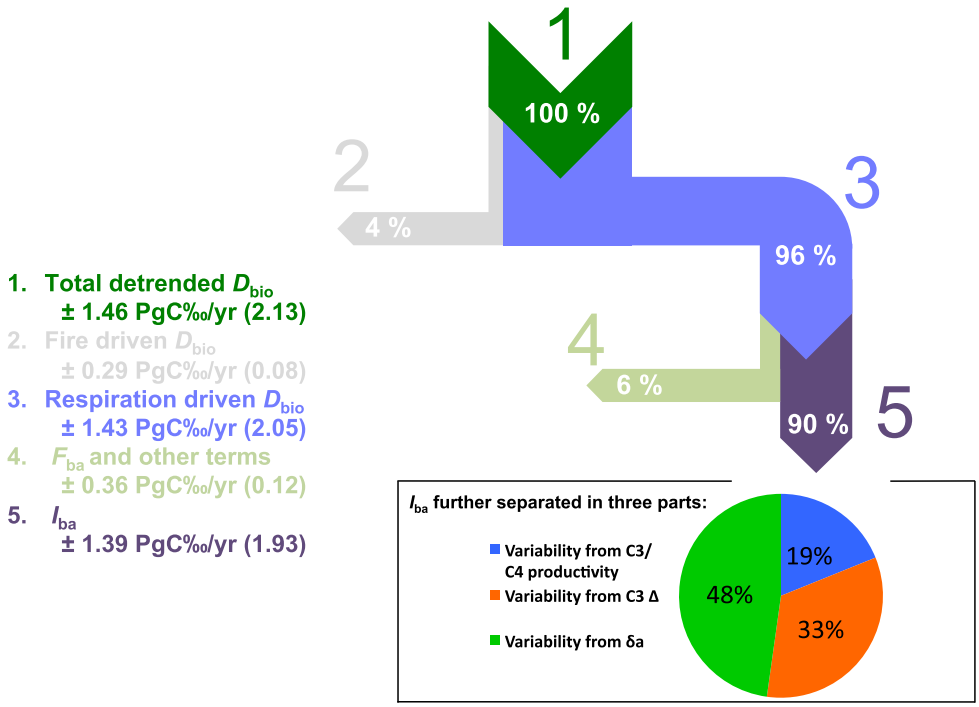

Figure 4. Schematic outcome of the important processes that are contributing to the total IAV in ISOVAR D_{bio} (2.13 [PgC‰yr^{-1}]^2, 1σ^2). Colors and percentages of the different components correspond with the summed areas in the covariance matrix in Figure 3. The numbered processes include 1σ standard deviation and 1σ^2 variance between parentheses. At the top of the figure, the total detrended variability in D_{bio}, which holds obviously 100% of the IAV, is separated into a respiration component (2.05/2.13 = 96% of total IAV) and a rest term that includes fire effects (0.08/2.13 = 4% of total IAV). The respiration component is further separated into contributions from $\overline{F_{ba}}I'_{ba}$ (1.93/2.13 = 90%) and $F'_{ba}\overline{I_{ba}}$ including other rest terms (0.12/2.13 = 6%). In $\overline{F_{ba}}I'_{ba}$, the fluctuations originate from three processes: variability in C_3/C_4 uptake ratio affecting global Δ (19%), variability in Δ_{C3} (33%), and variability in δ_a (48%). The variability from changes in C_3 and C_4 uptake was determined from the variance in the ISOFIX-FA simulation. The variability from Δ_{C3} was determined by taking the difference in variance between ISOVAR with the ISOFIX simulations. The δ_a variability was determined by comparing the variance of ISOFIX and ISOFIX-FA.

covariances instead of the 45% we would obtain if we used the GPP-Δ_{C3} dependence proposed by *Randerson et al.* [2002]. This raises an important question about whether the *Randerson et al.* [2002] hypothesis is realistic or whether the sensitivity of GPP and discrimination to climate variations is parameterized correctly in SiBCASA.

3.3. Variability in $\delta^{13}C$ Observations

[31] Looking at Table 2, the single largest number in the IAV budget of $\delta^{13}C$ is the variation in the growth rate itself (C_ad/dtδ_a). This number is the product of a very large atmospheric CO_2 abundance (C_a) and a small δ_a growth rate (d/dt). As a consequence, small errors in the growth rate of δ_a are strongly magnified in the final budget, and we will therefore look more closely at its uncertainty.

[32] The red line in the first two panels of Figure 5 shows the 17 year evolution of CO_2 and δ_a as determined from a set of 39 marine boundary layer (MBL) sites. The seasonal variations in CO_2 and δ_a clearly anticorrelate as summertime CO_2 uptake leaves the atmosphere heavier in ^{13}C, while on the decadal time scale the increase of CO_2 due to fossil fuel emissions causes an opposite trend in δ_a as isotopically light fossil fuel carbon (–28.6‰) is added. The annual growth rate for δ_a in the third panel is determined from difference between the first δ_a value of one year minus the first δ_a value of the previous year, as is commonly done. The similarity between the δ_a growth rate in the third panel and the isoflux term (C_ad/dtδ_a) in the fourth panel indicates that the IAV in the latter term is dominated by δ_a growth rate variations and not by C_a variability.

[33] To determine the uncertainty in the growth rate and atmospheric isoflux, we followed the bootstrapping procedure introduced by *Masarie and Tans* [1995] in which 100 alternative atmospheric monitoring configurations for the global network were used. Thereto, 39 random sites (with repetition) were drawn from the available network of 39 observing MBL sites and subsequently used to determine d/dtδ_a and C_ad/dtδ_a. We made sure that the random set of MBL sites specified for δ_a were identical to those for CO_2 for each bootstrap realization. This ensures that CO_2 and δ_a trends determined from each bootstrap run are comparable. This random selection of sites thus addresses the uncertainty

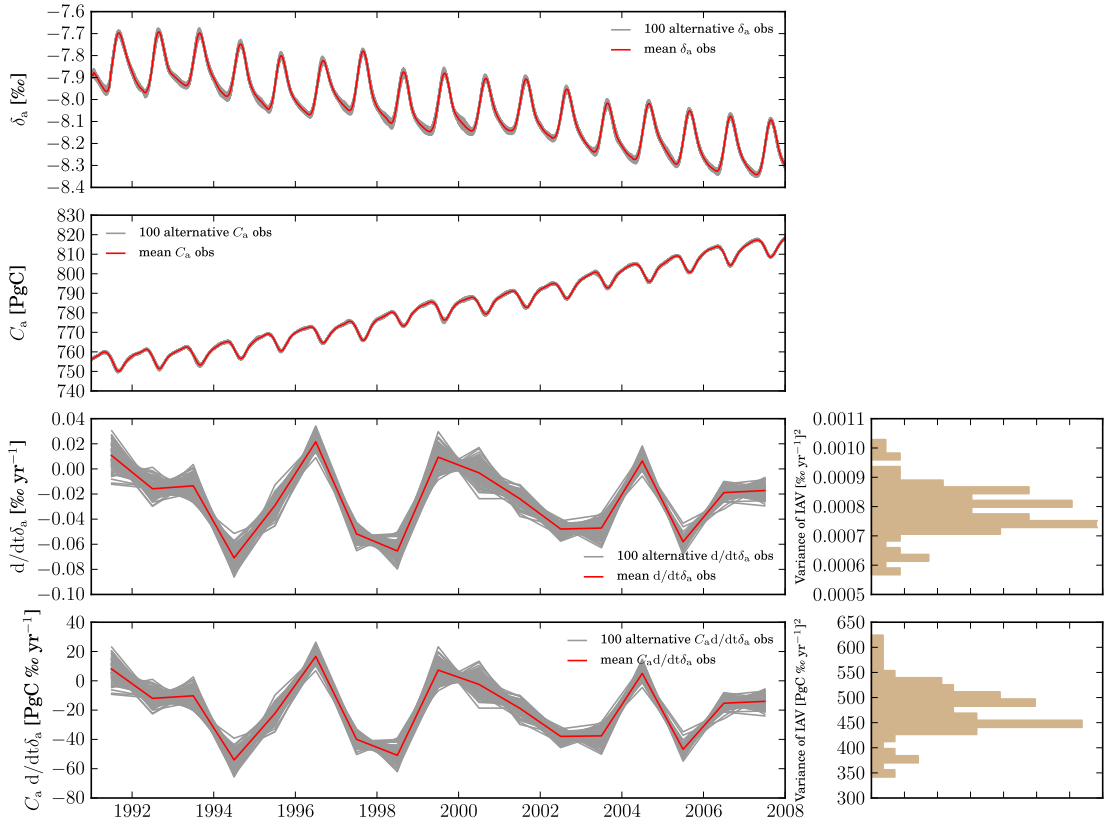

Figure 5. Four time series of δ_a, C_a, d/dtδ_a, and C_ad/dtδ_a. In the first panel, we displayed the 100 realizations of δ_a of the bootstrap analysis (gray) and the mean δ_a in ‰ (red). The same configuration is shown in the second panel but now for the atmospheric CO_2 content in PgC. By taking the first δ_a weekly value from one year minus the first weekly value of the previous year, we determined the mean (red) and each of the 100 (gray) d/dtδ_a and C_ad/dtδ_a, respectively. The last two panels are accompanied by a distribution histogram showing the IAV in $1\sigma^2$ ([‰yr^{-1}]^2 and [PgC‰yr^{-1}]^2) of each of the 100 realizations.

in the global C_ad/dtδ_a that results from an incomplete and uneven coverage of the globe by the network. The different growth rates resulting from this bootstrap analysis are shown graphically in the four panels in Figure 5 with the gray lines.

[34] When we next determine the IAV ($1\sigma^2$, over 17 years) in each of the 100 realizations, it is distributed like the histograms on the right-hand-side of the third and fourth panels. The mean of the 100 IAVs is around 450 [PgC‰yr^{-1}]^2, which is by definition the same as the IAV of the mean realization that was recorded in Table 2. But most importantly, we find that this IAV can deviate significantly and might be as small as 400 or or as big as 500 $\left[\text{PgC‰yr}^{-1}\right]^2$ within a 68% confidence interval. In other words, the IAV in the global growth rate of δ_a leaves significant room for smaller, or greater, atmospheric variability. This confidence interval is about 3 times larger than the calibration variability in δ_a measurements [*Alden et al.*, 2010].

[35] This result has possible consequences for our analysis of the IAV budget of δ_a. If the true atmospheric IAV is indeed toward the low end of our estimates (1σ: 20 PgC ‰ yr^{-1}, $1\sigma^2$: 400 [PgC‰yr^{-1}]^2), the residual IAV needed to close the budget would be only ±6.9 PgC ‰ yr^{-1} instead of our current 10.1 PgC ‰ yr^{-1} (see Table 2). The unexplained fraction of IAV to be projected onto net terrestrial and ocean CO_2 fluxes in a traditional double deconvolution with CO_2 and δ_a would thus be smaller and so would the IAV in the resulting fluxes. For the oceans, this would mean that atmospherically based estimates come in closer agreement with bottom-up ocean models, just like *Alden et al.* [2010] achieved with an IAV increase in disequilibrium fluxes. But also, net terrestrial CO_2 flux IAV would be lowered, bringing the large IAV (±1.6 PgC yr^{-1}) currently estimated in a double deconvolution a little bit closer (a reduction of ∼0.2 PgC yr^{-1} in standard deviation) to estimates based on CO_2 observations only (±1.2 PgC/yr). We note, however, that this sensitivity is not large enough to bring bottom-up modeling and single-deconvolution-based flux estimates in full agreement with the double deconvolution, as the latter still puts substantial amount of variability in N_{oce}. Also, the assumption that atmospheric IAV is lower than assumed can equally likely be replaced by the assumption that it is higher than assumed, until we investigate in more detail the ability of the current observing network to detect all variations in d/dtδ_a resulting from all terrestrial and ocean carbon exchange. Attempts to better interpret these variations are currently undertaken but beyond the scope of this work.

4. Discussion

4.1. Interannual Variability in Global $\delta^{13}C$ Budget Explained

[36] This study demonstrates a dichotomy between bottom-up and top-down estimates of the IAV of the disequilibrium flux. From a top-down perspective, a closed $\delta^{13}C$ budget with low variability in net ocean exchange can be achieved if a substantial fraction of IAV resides in the terrestrial disequilibrium flux ($\pm$12.5 PgC ‰ yr^{-1} in *Alden et al.* [2010]). However, the bottom-up simulated variability in the terrestrial disequilibrium flux, as calculated in this study, is 8 times smaller ($\pm$1.5 PgC ‰ yr^{-1}). Like in the studies of *Scholze et al.* [2003, 2008], our results suggest that IAV in C_3 discrimination (Δ_{C3}) is one of the drivers of the IAV in D_{bio}. As these two bottom-up terrestrial ^{13}C models agree on a rather small year-to-year variability in the global discrimination, our study suggests that other factors beside Δ_{C3} (such as underestimated variations in modeled C_3 and C_4 productivity) contribute substantially to the IAV in D_{bio} but are not nearly sufficient to produce the suggested $\pm$12.5 PgC ‰ yr^{-1} D_{bio} variations in *Alden et al.* [2010]. It is very well possible that the fractionation parameterization scheme used (including stomatal conductance) is lacking sensitivity to water stress. Further investigations of the sensitivity of stomatal conductance to atmospheric water vapor, radiation, and temperature need to be undertaken in the future, since these properties together have an effect on the isotopic fractionation. Additional sensitivity in Δ_{C3} could also depend on the chosen stomatal conductance formulation as shown by *Ballantyne et al.* [2010]. More IAV in either C_3/C_4 distributions or their relative responses to climate anomalies could invoke more IAV in global Δ, and thus indirectly in D_{bio} as well. So we either have to find our answers here or partly also in the other terms in the budget equation to explain the unaccounted fraction of variability.

[37] The traditional double deconvolution as presented under option (2) in section 3.1 and displayed in Figure 1b (dashed lines) deserves some further discussion. The suggestion that the mean residual can fairly easily be absorbed by D_{bio} or D_{oce} is already discussed in section 3.1 and in *Alden et al.* [2010]. As a result, the 17 year average land sink N_{bio} and ocean sink N_{oce} would remain unchanged: –3 and –2.1 PgC yr^{-1}, respectively. However, IAV in N_{bio} and N_{oce} increases considerably toward $\pm$1.6 and $\pm$0.9 PgC yr^{-1} with a strong anticorrelation as noted. The latter number for ocean IAV is not considered realistic based on recent ocean carbon exchange estimates [e.g., *Le Quere et al.*, 2007], but also the variability for biospheric exchange is higher than estimated by, for instance, CarbonTracker [*Peters et al.*, 2007]. The latter is based on CO_2 alone and could thus simply miss the information from $\delta^{13}C$, but first attempts suggest that also in a spatially explicit inversion of CO_2 and $\delta^{13}C$ in this framework, unrealistic IAV in ocean and terrestrial exchange deteriorates the results. Future $\delta^{13}C$ inversions, whether spatially explicit or based on double deconvolution, should therefore proceed with caution and carefully deal with other terms (D_{bio} and D_{oce}) when using atmospheric time series of multiyear time periods.

[38] One of the budget terms under investigation was the atmosphere. In section 3.3, we have seen that the constraint on the IAV of δ_a growth rate might not be as robust as previously thought. Out of the 100 realistic realizations of $C_a d/dt\delta_a$, we found a realistic spread of $\pm$50 $\left[\text{PgC‰yr}^{-1}\right]^2$ in the IAV, which is large compared to most variance terms in Table 2. One of the limitations of the network used is that the region with likely high isotopic variability is also the one that is least observed. Tropical carbon exchange is a strong mixture of C_3 and C_4 dominated species, and their signals are quickly transported from the surface to higher altitudes and hidden from the network for some time. Interannual variations in the vertical mixing strength would furthermore contribute to the signal that was remaining at the surface, but it cannot be accounted for in the global mass balance calculations presented here. Inclusion of vertical profile observations that are increasingly becoming available could help close the budget of $\delta^{13}C$ further. The large uncertainty on IAV in the atmospheric burden also poses the question whether previous carbon flux inversion studies that included atmospheric δ_a took the "lack of constraint" in observed IAV in consideration and as a result invoked too high IAV in the ocean and terrestrial net exchanges fluxes. However, it should be noted that our analysis of the ^{13}C growth rate uncertainty could just as likely enlarge the residual variance of 100 $\left[\text{PgC‰yr}^{-1}\right]^2$ as reduce it; the central value of IAV for the growth rate is still 450 $[\text{PgC‰yr}^{-1}]^2$.

[39] Could D_{oce} pose as another candidate for additional IAV? As in *Alden et al.* [2010], we assume that the ocean disequilibrium IAV is already reasonably described and an unlikely source for atmospheric ^{13}C variability. The small IAV of $\sim$2 $\left[\text{PgC‰yr}^{-1}\right]^2$ in the calculated value of D_{oce} (see Table 2 and Figure 4 in *Alden et al.* [2010]) results from interannual changes in both I_{oce} and F_{oa}. For I_{oce}(= $\delta_{oa} - \delta_{ao}$), δ_{ao} changes interannually purely as a function of declining δ_a. The δ_{oa} changes as a result of changing surface ocean ^{13}C of DIC, prescribed according to Figure 15 in *Gruber et al.* [1999]. The impact of changes in ^{13}C of DIC resulting from, e.g., reduction in upwelling waters in the eastern tropical Pacific during El Niño and the impact of sea surface temperature (SST) changes affecting the equilibrium fractionation factor [*Zhang et al.*, 1995] are neglected. F_{oa} is parameterized as a function of surface ocean pCO_2 and wind speed, after *Takahashi et al.* [2009]. Although pCO_2 is assumed to increase according to the atmospheric CO_2 trend, wind speed (and solubility) is assumed to be constant year to year. While there is some room for additional variability beyond what is specified, the argument put forward in section 3.2 that respiration variability is fundamentally limited by the large pool sizes from which it comes is even truer for the gross ocean to atmosphere flux. Uncertainty in the IAV of I_{oce} resulting from changes in ^{13}C of DIC are probably small because of the pool size effect. Sea surface temperatures can affect the equilibrium fractionation factor at a rate of 0.1‰/K [*Zhang et al.*, 1995]. In the ENSO regions, SST can change significantly, but these are also regions of low wind speed where F_{oa} (and thus D_{oce}) is likely to be small. Although the IAV of D_{oce} deserves more rigorous treatment, we feel it is an unlikely candidate to explain the residual variance in Table 2.

[40] Fires likely contribute more to IAV in the CO_2 and $C_a d/dt\delta_a$ records than currently modeled in SiBCASA. The IAV in the recent GFED3-CASA fire estimates [*van der Werf et al.*, 2010], which does include the El Niño 1997–1998

peak of 2.8 PgC/yr, has an IAV of 0.37 PgC yr^{-1}. In the $C_a d/dt \delta_a$ budget, it comes down to an IAV of 5.6 PgC ‰ yr^{-1} (30 [PgC‰yr^{-1}]^2). This is obviously larger than the SiBCASA estimates (2.3 PgC ‰ yr^{-1}); however, it is not enough to account for the whole residual term (100 [PgC‰yr^{-1}]^2).

[41] Another potential candidate that can account for the unexplained fraction of variability is the fossil fuel isoflux. If we assume ±0.2 PgC yr^{-1} as a realistic uncertainty in F_{ff} and prescribe this as IAV, we need an IAV of ±1.3‰ (1σ) in global mean δ_{ff} to produce a fossil fuel isoflux with enough IAV to close the variability gap. But is such an IAV in δ_{ff} realistic? The total yearly isotopic ratio δ_{ff} can be separated into contributions from different fuel types, where each type has its own characteristical range of isotopic signatures, i.e., $\delta_{ff} = \left(F_{coal}\delta_{coal} + F_{oil}\delta_{oil} + F_{gas}\delta_{gas}\right)/F_{ff}$. The signatures themselves have uncertainties, but δ_{coal} and δ_{oil} are known to be within 1–2‰. The isotopic composition of natural gas is much more variable, and even within a single production field the isotopic signature can vary widely. The global average isotopic signature for natural gas is typically –44‰, while odd deviations exist if natural gas is either associated with coal or with marine sediments (–20 or –100‰, respectively [*Andres et al.*, 2000]). This makes the estimation of global weighted averages difficult [*Andres et al.*, 2000], and in that light, varying contributions to the global total fossil fuel mixture by natural gas of varying isotopic signatures could provide additional IAV. Interestingly, in the past when F_{ff} was 4 or 5 PgC yr^{-1}, both uncertainty and variability in δ_{ff} was only half as important as it is today.

4.2. Assessment ^{13}C Model Framework

[42] The LPJ adaptation of *Scholze et al.* [2003, 2008] is one of the few models available to compare our ^{13}C framework with. Even though observed GPP at flux towers indicates that SiBCASA performs better overall than LPJ (K. Schaefer, personal communication, 2011), the overall results in Δ and disequilibrium flux are similar. We, however, observe in Δ a much greater contribution from changes in C_3 and C_4 productivity rather than from changes in the fractionation factor. This difference primarily stems from the amount of C_4 photosynthesis: where *Scholze et al.* [2003] lacks C_4 land use (pastures and crops) and, hence, assigns less than 10% of the total photosynthesis to C_4 GPP, we assign 30%, which acts more heavily on the assimilated weighted value of Δ.

[43] Another disparity between the models is the different explanations for the long-term trends of Δ observed in ISOVAR. Both models show an increase of 0.3–0.5‰ in discrimination over the course of the 20th century. We found that (1) long-term increases in C_3 GPP at the expense of C_4 GPP forced the global plant discrimination to rise and (2) increases in atmospheric CO_2 raised the chloroplast-atmosphere CO_2 ratio and subsequently raised the C_3 plant discrimination factor at leaf level. *Scholze et al.* [2003] ascribes the trend mainly to the response of plants to increased water stress. In our study, long-term changes in the meteorological forcing were not included, which could have added up as an additional effect on the Δ trend.

[44] The differences in ISOVAR disequilibrium isoflux between *Scholze et al.* [2008] (34.8 PgC ‰ yr^{-1}) and this study (25.4 PgC ‰ yr^{-1}) at the end of the simulation period is most likely a consequence of differences in heterotrophic respiration fluxes (69.4 PgC yr^{-1} compared to 52.3 PgC yr^{-1} in our study). Globally, the average disequilibrium forcing coefficient I_{ba} was estimated at 0.23‰ for 1991–2007. This coefficient being scaled with the autotrophic and heterotrophic respiration flux (total 110 PgC yr^{-1}) and a small flux due to biomass burning gives a disequilibrium flux and IAV of 25.4 ± 1.5 PgC ‰ yr^{-1}. If we would base D_{bio} solely on heterotrophic respiration, as done in most other studies, I_{ba} would become 0.48‰, and D_{bio} would become 24.9 ± 1.1 PgC ‰ yr^{-1}. Note that IAV in D_{bio} would even be smaller. These results compared well with other experiments. In 1988 (for comparison), I_{ba} was estimated at 0.42‰ if it would be based on heterotrophic respiration. This value lies in the middle to the ones found elsewhere for the same year. For example, *Joos and Bruno* [1998] reported 0.43‰, *Scholze et al.* [2008] reported 0.59‰, *Alden et al.* [2010] reported 0.40‰, and *Fung et al.* [1997] reported 0.33‰. *Tans et al.* [1993] reported 0.20‰ as an average for the period 1970–1990. Even so, toward the atmosphere, the low values of our I_{ba} were compensated by a larger respiration flux (heterotrophic + autotrophic), thus maintaining a similar disequilibrium flux D_{bio} with other published experiments.

5. Conclusion

[45] To conclude, we answer our main research questions:

[46] 1. Our new terrestrial bottom-up results cannot confirm the suggestion of a closed $\delta^{13}C$ budget that allows low prescribed ocean net exchange variability. Because our model calculates low interannual variability in terrestrial disequilibrium flux, it suggests that other terms in the mass balance must accommodate the unaccounted variability. We identify several possible candidates: the atmospheric term, the fossil fuel emissions, and the terrestrial CO_2 net exchange term. Considering that we underestimate the IAV in forest fires, it could also explain a portion of the necessary leverage.

[47] 2. We found that C_3 GPP and Δ_{C3} do covary as suggested by *Randerson et al.* [2002], but their contribution to the variance in the C_3-only uptake isoflux is rather small (10%).

[48] 3. And finally, we found that variations in Δ_{C3}, C_3, and C_4 productivity and δ_a are the main drivers of variability in the disequilibrium flux. Fire and respiration variations play a minor role. We cannot rule out the possibility of more variability in globally averaged plant discrimination, either as a result of higher C_3 discrimination sensitivity to water stress than parameterized in the model or more IAV in either C_3/C_4 distributions or their relative responses to climate anomalies.

[49] **Acknowledgments.** The authors are most grateful to Caroline Alden for her support and provision of data. We further wish to thank the benefactors and colleagues that are participating in the Netherlands-China Exchange Program. Ivar van der Velde was supported by a VIDI grant (project 5120490-01) provided by the Netherlands Organization for Scientific Research (NWO). Wouter Peters was supported by the Geocarbon project. The measurements of CO_2 and $\delta^{13}C$ used in this publication were supported by NOAA Earth System Research Laboratory and Climate Program Office.

References

Alden, C. B., J. B. Miller, and J. W. C. White (2010), Can bottom-up ocean CO_2 fluxes be reconciled with atmospheric ^{13}C observations? *Tellus, Ser. B*, *62*(5), 369–388, doi:10.1111/j.1600-0889.2010.00481.x.

Andres, R. J., G. Marland, T. A. Boden, and S. Bischof (2000), Carbon dioxide emissions from fossil fuel consumption and cement manufacture, 1751–1991, and an estimate of their isotopic composition and latitudinal distribution, in *The Carbon Cycle*, edited by Wigley, T., and D. Schimel, pp. 53–62, Cambridge Univ. Press, Oxford, U. K.

Ballantyne, A. P., J. B. Miller, and P. P. Tans (2010), Apparent seasonal cycle in isotopic discrimination of carbon in the atmosphere and biosphere due to vapor pressure deficit, *Global Biogeochem. Cycles*, *24*, GB3018, doi:10.1029/2009GB003623.

Boden, T. A., G. Marland, and R. J. Andres (2009), Global, regional, and national fossil-fuel CO_2 emissions*, Carbon Dioxide Inf. Anal. Cent., Oak Ridge Natl. Lab., U.S. Dep. of Energy, Oak Ridge, Tenn.* doi:10.5194/acp-10-11707-2010.

Ciais, P., P. P. Tans, J. White, and M. Trolier (1995), Partitioning of ocean and land uptake of CO_2 as inferred by $\delta^{13}C$ measurements from the NOAA Climate Monitoring and Diagnostics Laboratory Global Air Sampling Network, *J. Geophys. Res.*, *100*, 5051–5070.

Collatz, G. J., J. Ball, C. Grivet, and J. A. Berry (1991), Physiological and environmental regulation of stomatal conductance, photosynthesis and transpiration - a model that includes a laminar boundary layer, *Agric. For. Meteorol.*, *54*, 107–136.

Collatz, G. J., M. Ribas-Carbo, and J. A. Berry (1992), Coupled photosynthesis-stomatal conductance model for leaves of C4 plants, *Aust. J. Plant. Physiol.*, *19*(5), 519–538.

Farquhar, G. D. (1983), On the nature of carbon isotope discrimination in C4 species, *Aust. J. Plant Physiol.*, *10*(1), 205–226.

Farquhar, G. D., S. V. Caemmerer, and J. A. Berry (1980), A biochemical-model of photosynthetic CO_2 assimilation in leaves of C3 species, *Planta*, *149*(1), 78–90.

Francey, R. J., P. P. Tans, C. E. Allison, I. G. Enting, J. W. C. White, and M. Trolier (1995), Changes in oceanic and terrestrial carbon uptake since 1982, *Nature*, *373*(6512), 326–330.

Francey, R. J., C. E. Allison, D. M. Etheridge, C. M. Trudinger, I. G. Enting, M. Leuenberger, R. L. Langenfelds, E. Michel, and L. P. Steele (1999), A 1000-year high precision record of delta C-13 in atmospheric CO_2, *Tellus, Ser. B*, *51*, 170–193.

Fung, I., et al. (1997), Carbon 13 exchanges between the atmosphere and biosphere, *Global Biogeochem. Cycles*, *11*(4), 507–533.

Giglio, L., J. T. Randerson, G. R. van der Werf, P. S. Kasibhatla, G. J. Collatz, D. C. Morton, and R. S. DeFries (2010), Assessing variability and long-term trends in burned area by merging multiple satellite fire products, *Biogeosciences*, *7*(3), 1171–1186.

Gruber, N., C. D. Keeling, R. B. Bacastow, P. R. Guenther, T. J. Lueker, M. Wahlen, H. A. J. Meijer, W. G. Mook, and T. F. Stocker (1999), Spatiotemporal patterns of carbon-13 in the global surface oceans and the oceanic Suess effect, *Global Biogeochem. Cycles*, *13*(2), 307–335.

Joos, F., and M. Bruno (1998), Long-term variability of the terrestrial and oceanic carbon sinks and the budgets of the carbon isotopes C-13 and C-14, *Global Biogeochem. Cycles*, *12*(2), 277–295.

Kaplan, J. O., I. C. Prentice, and N. Buchmann (2002), The stable carbon isotope composition of the terrestrial biosphere: Modeling at scales from the leaf to the globe, *Global Biogeochem. Cycles*, *16*(4), 1060, doi:10.1029/2001GB001403.

Le Quere, C., et al. (2003), Two decades of ocean CO_2 sink and variability, *Tellus, Ser. B*, *55*(2), 649–656.

Le Quere, C., et al. (2007), Saturation of the southern ocean CO_2 sink due to recent climate change, *Science*, *316*, 1735–1738.

Lloyd, J., and G. D. Farquhar (1994), $^{1}3C$ discrimination during CO_2 assimilation by the terrestrial biosphere, *Oecologia*, *99*, 201–215.

Masarie, K. A., and P. P. Tans (1995), Extension and integration of atmospheric carbon-dioxide data into a globally consistent measurement record, *J. Geophys. Res.*, *100*(D6), 11,593–11,610.

Page, S. E., F. Siegert, J. O. Rieley, H. D. V. Boehm, A. Jaya, and S. Limin (2002), The amount of carbon released from peat and forest fires in Indonesia during 1997, *Nature*, *420*, 61–65, doi:10.1038/nature01131.

Peters, W., et al. (2007), An atmospheric perspective on North American carbon dioxide exchange: CarbonTracker, *Proc. Natl. Acad. Sci. U. S. A.*, *104*, 18,925–18,930.

Randerson, J. T., M. V. Thompson, C. M. Malmstrom, C. B. Field, and I. Y. Fung (1996), Substrate limitations for heterotrophs: Implications for models that estimate the seasonal cycle of atmospheric CO_2, *Global Biogeochem. Cycles*, *10*(4), 585–602.

Randerson, J. T., G. J. Collatz, J. E. Fessenden, A. D. Munoz, C. J. Still, J. A. Berry, I. Y. Fung, N. Suits, and A. S. Denning (2002), A possible global covariance between terrestrial gross primary production and ^{13}C discrimination: Consequences for the atmospheric ^{13}C budget and its response to ENSO, *Global Biogeochem. Cycles*, *16*(4), 1136, doi:10.1029/2001GB001845.

Rayner, P. J., R. M. Law, C. E. Allison, R. J. Francey, C. M. Trudinger, and C. Pickett-Heaps (2008), Interannual variability of the global carbon cycle (1992–2005) inferred by inversion of atmospheric CO_2 and delta(CO_2)-C-13 measurements, *Global Biogeochem. Cycles*, *22*(3), GB3008, doi:10.1029/2007GB003068.

Reynolds, O. (1895), On the dynamical theory of incompressible viscous fluids and the determination of the criterion, *Philos. Trans. R. Soc.*, *186*, 123–164.

Schaefer, K., G. J. Collatz, P. P. Tans, A. S. Denning, I. Baker, J. A. Berry, L. Prihodko, N. Suits, and A. Philpott (2008), Combined simple Biosphere/Carnegie-Ames-Stanford approach terrestrial carbon cycle model, *J. Geophys. Res.*, *113*, G03034, doi:10.1029/2007JG000603.

Scholze, M., J. O. Kaplan, W. Knorr, and M. Heimann (2003), Climate and interannual variability of the atmosphere-biosphere $^{13}CO_2$ flux, *Geophys. Res. Lett.*, *30*(2), 1097, doi:10.1029/2002GL015631.

Scholze, M., P. Ciais, and M. Heimann (2008), Modeling terrestrial ^{13}C cycling: Climate, land use and fire, *Global Biogeochem. Cycles*, *22*, GB1009, doi:10.1029/2006GB002899.

Sellers, P. J., D. A. Randall, G. J. Collatz, J. A. Berry, C. B. Field, D. A. Dazlich, C. Zhang, G. D. Collelo, and L. Bounoua (1996), A revised land surface parameterization (SiB2) for atmospheric GCMs. Part I: Model formulation, *J. Clim.*, *9*(4), 676–705.

Still, C. J., J. A. Berry, G. J. Collatz, and R. S. DeFries (2003), Global distribution of C-3 and C-4 vegetation: Carbon cycle implications, *Nat. Clim. Change*, *17*, 1006–1019.

Suess, H. E. (1955), Radiocarbon concentration in modern wood, *Science*, *122*(3166), 415–417.

Suits, N., A. Denning, J. Berry, and C. Still (2005), Simulation of carbon isotope discrimination of the terrestrial biosphere, *Global Biogeochem. Cycles*, *19*, GB1017, doi:10.1029/2003GB002141.

Takahashi, T., et al. (2009), Climatological mean and decadal change in surface ocean pCO(2), and net sea-air CO_2 flux over the global oceans, *Deep Sea Res. Part II*, *56*(8–10), 554–577, doi:10.1016/j.dsr2.2008.12.009.

Tans, P. P. (1980), On calculating the transfer of C-13 in reservoir models of the carbon-cycle, *Tellus*, *32*(5), 464–469.

Tans, P. P., J. A. Berry, and R. F. Keeling (1993), Oceanic $^{13}C/^{13}C$ observations—A new window on ocean CO_2 uptake, *Global Biogeochem. Cycles*, *7*(2), 353–368.

van der Werf, G. R., J. T. Randerson, G. J. Collatz, and L. Giglio (2003), Carbon emissions from fires in tropical and subtropical ecosystems, *Global Change Biol.*, *9*(4), 547–562.

van der Werf, G. R., et al. (2010), Global fire emissions and the contribution of deforestation, savanna, forest, agricultural, and peat fires (1997–2009), *Atmos. Chem. Phys.*, *10*(23), 11,707–11,735, doi:10.5194/acp-10-11707-2010.

Winguth, A. M. E., M. Heimann, K. D. Kurz, E. Maierreimer, U. Mikolajewicz, and J. Segschneider (1994), El-Nino-southern oscillation related fluctuations of the marine carbon-cycle, *Global Biogeochem. Cycles*, *8*(1), 39–63.

Zhang, J., P. D. Quay, and D. O. Wilbur (1995), Carbon-isotope fractionation during gas-water exchange and dissolution of CO_2, *Geochim. Cosmochim. Acta*, *59*(1), 107–114, doi:10.3334/CDIAC/00001.